ACS Sustainable Chemistry & Engineering

pubs.acs.org/journal/ascecg

Research Article

Multiscale Study of Functional Acetylation of Cellulose Nanomaterials by Design: *Ab Initio* Mechanisms and Chemical Reaction Microkinetics

Ana Oberlintner, Matej Huš, Blaž Likozar, and Uroš Novak*

Cite This: *ACS Sustainable Chem. Eng.* 2022, 10, 15480−15489

Read Online

ACCESS | Metrics & More | Article Recommendations | Supporting Information

ABSTRACT: Cellulose nanomaterials, namely cellulose nanocrystals (CNCs) and cellulose nanofibrils (CNFs), present a class of multipurpose, renewable, biodegradable, and nontoxic materials, paving the way into the future of biobased materials. The abundance of hydroxyl groups on the surface allows modification of the materials properties according to application; however, to fully exploit their potential, better compatibility on the molecular level with the hydrophobic matrixes has to be explored beyond lab scale. One of the main missing pieces in functionalization of nanomaterials is a lack of studies focusing on mechanisms and kinetics, which are prerequisite for further optimization of conditions leading to optimal process in terms of both sustainable processing and optimal performance. In this study, the "by design" based approach to tailor biomaterial properties has been simulated multiscale-wise, thus providing a greatly needed input for commercialization. The microkinetic parameters of the elementary reaction steps for acetylation of two distinct types of cellulose nanomaterials were determined and refined by regression analysis. *Ab initio* part utilizes the density functional theory (DFT) for cellotriose as a model, which suggested that products were obtained through a mechanism consisting of active intermediate formation/subsequent competing one- or two-step (through binding/decomposition of complex) reactions. Quantum chemical simulations were used to pinpoint the most probable sequence through calculated activation barriers that served as a foundation for the development of a thorough regression analysis on experimental data sets. The yield of reaction, through formed acetyl groups was determined through Fourier transform infrared spectroscopy, leading to acquisition of critical elementary characteristics.

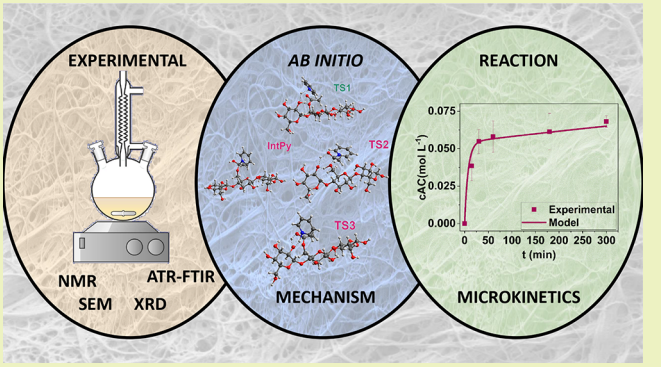

KEYWORDS: *cellulose, esterification, hydrophobicity, chemical reaction mechanism, density functional theory, multiscale microkinetic modeling*

INTRODUCTION

Produced by plants through the process of photosynthesis, cellulose takes the place as the most abundant polymer in nature, and is as such readily available worldwide to be used in various applications. Besides economic feasibility, its further advantages are biodegradability, nontoxicity, biocompatibility, and the possibility to extract particles of nanoscale.[1] Cellulose nanocrystals (CNCs) are, as defined by The American Paper & Pulp Association (TAPPI WI 3021), nanoparticles with pure crystalline structure measuring up to 3−10 nm in width and with an aspect ratio larger than 5, however usually less than 50.[2] 2,2,6,6-Tetramethylpiperidine-1-oxyl radical(TEMPO)-mediated oxidation of cellulose biomass coupled with mechanical treatment yields cellulose nanofibrils (CNFs), which are in the form of long fibrilous networks with a diameter of individual fibril up to 100 nm and length up to a few micrometers.[3] The backbone of cellulose nanomaterials consists of anhydroglucose units (AGUs) alternately rotated around their axis for 180° and linked by β-glycosidic bonds which are, along with hydrogen bonds, the reason behind cellulose's rigidity, stiffness, high mechanical strength, and crystalline character.[4] There are two proposed models defining the distribution of ordered (crystalline) and disordered (amorphous) regions in cellulose: (a) it can be described as an alternation of the crystalline and amorphous domains along the biopolymer fiber, where the amorphous domains are placed between the crystalline regions as a result of internal strain causing the fiber to tilt and twist,[5] or (b) such defects are not

Received: August 5, 2022
Revised: October 25, 2022
Published: November 9, 2022

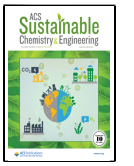

fully amorphous; however, at the twists and sharp bends of the fiber, its core remains crystalline and the disordered regions are present only on the surface.[6,7]

Along with other nanofibers, cellulose nanomaterials are heavily investigated as a filler for polymers or biopolymers, especially by researchers in the wood and paper industry as well as groups dealing with biomaterials.[8] Potential applications of cellulose/polymer nanocomposite are rising due to its truly sustainable character and abundance, and it has achieved a status of a "new" class of materials for use in various fields including thermosets used for packaging, automobile, electronics, textile, construction, medical devices, and many more. In terms of processing cellulose nanocomposites, almost half of the published research reports the use of solvent casting method, which is not easily industrially scalable.[9] In a conventional industrial setting, fibers and thermoplastics are melt mixed to generate compounds, followed by profile extrusion, compression molding, or injection molding processes to yield composite products at high production rates. There are several processing challenges and sustainability issues involved in applying cellulose nanomaterials into conventional and biobased thermoplastic processing systems.[10] The latter is related to the greener chemistry of cellulose functionalization and diminishing the environmental footprint of the chemicals but also to improving the economic feasibility.[11] To overcome the dispersion of cellulose nanomaterials in thermoplastic (bio)polymers solution, both a nanocellulose treatment chemically or physical surface treatments have been demonstrated as an efficient option, thus potentially boosting the industrial applications.[12] Hydroxyl groups on the surface allow a vast range of surface modifications[13] that can overcome the weakness posed by hydrogen bonding causing limited compatibility with polymer matrices,[14] but it has to be taken into account that among the three hydroxyl groups on the surface of a monomeric unit, not all of them are equally reactive and susceptible to functionalization. The hydroxyl group on the C6 position (using conventional numbering with C1 being the anomeric carbon) is much more reactive than C2- or C3-bound hydroxyl groups. Additionally, modification of only the C6-bound group does not interfere with the mechanical strength of cellulose fibers, leading to recent efforts of regioselective acetylation.[15,16] An overview of hydrophobization methods on cellulose nanomaterials shows esterification is the favored way of minimizing the hydrophilic effect,[15,17] with acetylation being one of the most widely used cellulose modifications that has also been commercially utilized in a number of applications and can be translated to the nanoscale, as well. Commercial cellulose acetylation is carried out with sulfuric acid as a catalyst, but the process is environmentally problematic and presents a health hazard, prompting research in better substitutes. Alternatively, acetylation of CNCs using acetic anhydride in various media, such as citric acid and pyridine, has been described by several authors.[17,18] Acetylation of cellulose nanomaterials was shown to improve dispersibility in common solvents as well as polymer matrices. In practical applications, the result of modification was an increase in mechanical strength of PLA-based polymers with integrated acetylated cellulose nanomaterials, due to better compatibility as a result of surface hydrophobicity.[18,19] Furthermore, acetylated CNCs were demonstrated to improve the toughness of a vitrimer upon their incorporation.[20] Due to their fibrilous structure, acetylated CNFs were successfully (as opposed to pristine CNFs) utilized as Pickering emulsion stabilizers.[21] Despite their huge potential, cellulose nanomaterials are not utilized on the industrial scale yet, due to several limitations that are well described by Wang et al.[12] The industrialization of these materials depends on solving problems regarding both processing techniques and surface modification.

While a number of studies inspected possible routes to esterification of cellulose nanomaterials and their practical applications, only a limited number of them focused on the reaction mechanisms and kinetics.[22] Several authors have investigated the kinetic of wood acetylation with acetic anhydride, assuming either a one-step (direct acetylation of hydroxyl groups) or a two-step mechanism (including dissolution of sulfated chains), with reaction kinetics following a pseudo-first-order expression.[23−26] To be able to evaluate the economic feasibility and sustainability of acetylated nanomaterials and promote their wider use in commercial applications, this precise knowledge is needed as demonstrated by Kanematsu et al.[27]

With this in mind, the present study revisits the investigation of pyridine-mediated acetylation with acetic anhydride mechanisms and kinetics on two types of cellulose nanomaterials (CNCs and CNFs). A revised mechanism of cellulose nanomaterials acetylation consisting of several routes is hypothesized. *Ab initio* calculations should provide an insight into the atomistic mechanism through the determination of activation barriers. The subsequent microkinetic modeling, supported by experiments under various conditions (temperatures in the range from 60 to 90 °C and varying reactant ratios), can confirm the preliminary hypothesis. Additionally, in the frame of experimental investigation, the chemical and morphological characterization of the cellulose derivatives was carried out using ATR-FTIR, phosphorus-31 NMR, solid-state NMR, XRD, and SEM. The final hypothesis aims to confirm that the developed microkinetic model can describe the acetylation reaction for CNCs as well as CNFs.

EXPERIMENTAL SECTION

Materials. CNFs (Valida S, 3% wt. suspension) was supplied by Sappi (Maastricht, Netherlands), and CNCs were purchased from Navitas (Stari trg pri Ložu, Slovenia). For acetylation of cellulose nanomaterials, the following chemicals were used: toluene (Honeywell), pyridine (Merck), acetic anhydride and acetone (Sigma-Aldrich). For NMR analyses, deuterated chloroform, chromium(III) acetylacetonate (relaxation agent), and 2-chloro-4,4,5,5- tetramethyl-1,2,3-dioxophospholane (TMDP) were all purchased from Sigma-Aldrich, while the internal standard *N*-hydroxy-5-norbornene-2,3-dicarboxylic acid imide (NHND, > 99%) was purchased from Tokyo Chemical Industry.

Methods. *Characterization Pristine and Modified Cellulose Nanomaterials.* To ascertain the morphology, approximately 100 mg of cellulose nanomaterial dispersion in water (approximately 3 wt %) was diluted in 5 mL of acetone. A few drops of cellulose nanomaterial−acetone solution were added onto the surface of a heated sample holder, which was previously smoothed with sand paper, to quickly evaporate the solvent. The sample was then inspected as is with scanning electron microscope SUPRA 35VP (Carl Zeiss, Jena, Germany) at near-vacuum conditions. For TEM analysis, 10 mg of cellulose nanomaterial was dispersed in 20 mL of acetone and analyzed using JEOL ARM 200F electron microscope (JEOL, Akishima, Japan). The size of the nanoparticles was determined from the TEM micrograph from at least 25 points with ImageJ software, and the average is reported.

The amount of accessible hydroxyl groups on the surface of pristine nanocellulose was assessed by measuring ^{31}P with Bruker Avance Neo 600 MHz NMR spectrometer (Bruker, Germany). TMDP was

https://doi.org/10.1021/acssuschemeng.2c04686
ACS Sustainable Chem. Eng. 2022, 10, 15480−15489

reacted with freeze-dried and vacuumed CNCs and CNFs for 30 min in the presence of the internal standard (NHND), following the protocol proposed by Brand et al.[28] The amount of accessible groups was calculated from the peak integrals of the unreacted TMDP, internal standard NHND, and water. The amount of surface hydroxyl groups was also calculated theoretically through the crystallite size.

^{13}C cross-polarization/magic-angle spinning (^{13}C CP/MAS) solid state NMR spectra were recorded on Bruker Avance Neo 400 MHz NMR spectrometer (Bruker, Germany) equipped with a 4 mm HX MAS probe. The analysis was done at a spinning rate of 15 kHz.

To evaluate the crystallinity, the freeze-dried samples of CNCs were analyzed directly, while CNFs had to be flattened by pressure once dry as described by Peng et al.[29] to be suitable for analysis. Before the analysis they were fixed on modeling clay. The XRD spectra were recorded with the PANanalytical X'Pert PRO (Malvern Panalytical, UK) high-resolution diffractometer using Cu Kα radiation (1.5406 Å) in a 2θ range from 5° to 59° (100 s per step 0.034°). The crystallinity index CrI was calculated by the Segal method:[30]

$$\mathrm{CrI} = \frac{I_{200} - I_{\mathrm{am}}}{I_{200}} 100 \quad (1)$$

where I_{200} is the maximum intensity of the diffraction from the crystalline (200) plane at 2θ = 22.8° and I_{am} is the minimum intensity of the amorphous region measured at 2θ = 18°. Crystallite size (C_A) was calculated based on the obtained XRD spectra following eq 2.

$$C_A = \frac{K\lambda}{\beta \cos 2\theta} \quad (2)$$

where K is 1 (the Scherrer constant for needle-like crystallites) and λ is the used wavelength (0.15406 nm). β is the width of half-maximum of the diffraction peak angle of the (002) crystal plane. β is expressed in radians, while 2θ is in degrees.[31] The amount of surface chains (R) proportional to total amount of chains was calculated using lattice plane d-spacings of the cellulose I monoclinic unit cell.[28]

The freeze-dried samples were measured with FT-IR Spectrum Two (PerkinElmer, Waltham, USA) instrument in a range of wavelengths of 4000−400 cm^{-1} with 64 scans with increments (resolution) of 4 cm^{-1}. The spectra were adjusted to the same baseline and normalized to the C−O peak at 1056 cm^{-1} that is a characteristic peak for a cellulose backbone and is not altered by the reaction. The acetyl content is calculated through the $I_{C=O}$ and I_{C-O} ratio as stated in the literature.[32] The accuracy of the method was assessed through titration (Supporting Information).

Acetylation of Cellulose Nanomaterials. CNCs and CNFs were acetylated according to a modified protocol by Lin et al.[18] The detailed description of the procedure can be found in the Supporting Information. The reaction conditions are summarized in Table 1, with additionally tested parameters in Table S1.

Quantum Chemical Simulations. DFT calculations served to study the reaction mechanism. Electronic structures were calculated with NWChem 6.8.[33] Within the linear combination of atomic orbitals method, we used a hybrid functional (M06-2X)[34] with Pople's basis set 6-31+G(d) for optimization and TS search[35−38] and 6-311++G(d,p) for single-point energy calculations, which is known to reproduce the main group thermochemistry sufficiently well.[39] Solvation was modeled implicitly with the solvation model based on density (SMD)[40] with the default values for pyridine (dielectric constant: 12.978). Benchmark calculations were also done using toluene (dielectric constant: 2.4) to evaluate the effect of adding toluene, which was necessary for CNFs.

Structural optimization was performed until the forces dropped below 1.5 × 10^{-5} hartree/bohr. The structures were characterized with vibrational analysis to differentiate between stable and saddle points. The transition states were identified using the climbing image nudged elastic band method[41] and confirmed by IRC.

Modeling. *The Quantum Model.* Cellulose is a prohibitively large system to be described by contemporary quantum chemistry methods. Ponnuchamy et al.[42] have already shown that cellobiose can be used as a model compound for studying wood modification with acetic anhydride. Due to the computational power available, we use cellotriose (an oligomer of three *D*-glucose units) in the most stable tg configuration[43] as a model, as shown in Figure S1. This structure is large enough to allow for the cooperation of neighboring monomeric units (see the mechanism below) and reproduces the steric hindrance brought about by a chain of monomeric units, yet small enough to be computationally tractable. Acetic anhydride was modeled as the acetylating agent.

With large molecules, several local minima exist. To find the lowest-lying initial structure, several different relative positions were tested. Upon structural relaxation, each geometry was slightly perturbed and subjected to first-principles molecular dynamics to locate any adjacent lower minima. Moreover, after any transition state was located, a full IRC descent to the reactants was performed and further optimized. Herein, we present only global minima for the reactants, intermediates, and products.

The Microkinetic Model. The DFT-obtained reaction parameters for the reaction mechanism were cast in the microkinetic model, which assumed the following:

- negligible side reactions
- homogeneously stirred reaction mixture
- a fraction of equally reactive surface hydroxyl groups available for reaction (determined experimentally)
- batch mode operation of the ideal reactor
- no mass transfer limitations

A system of differential equations (dc/dt) describing the concentration profiles of each reaction step was solved as described in the Supporting Information, using the DFT-obtained parameters for the Arrhenius-like kinetics.

Table 1. Tested Experimental Conditions

Experiment No.	T (°C)	AGU:Pyridine:Acetic Anhydride (mol)
	CNC	
1.1	60	1:10:8.56
1.2	60	1:30:8.56
1.3	60	1:50:8.56
1.4	70	1:10:8.56
1.5	70	1:30:8.56
1.6	70	1:50:8.56
1.7	80	1:20:8.56
1.8	80	1:30:8.56
1.9	80	1:40:8.56
1.10	80	1:50:8.56
1.11	90	1:8.6:8.6
1.12	90	1:10:8.56
1.13	90	1:30:6.00
1.14	90	1:30:8.56
1.15	90	1:40:8.56
1.16	90	1:50:8.56
	CNF	
2.1	60	1:10:8.56
2.2	60	1:30:8.56
2.3	70	1:30:8.56
2.4	70	1:40:8.56
2.5	80	1:10:8.56
2.6	80	1:30:4.82
2.7	80	1:30:8.56
2.8	80	1:40:8.56
2.9	80	1:50:8.56
2.10	90	1:10:8.56
2.11	90	1:30:8.56
2.12	90	1:40:8.56

https://doi.org/10.1021/acssuschemeng.2c04686
ACS Sustainable Chem. Eng. 2022, 10, 15480−15489

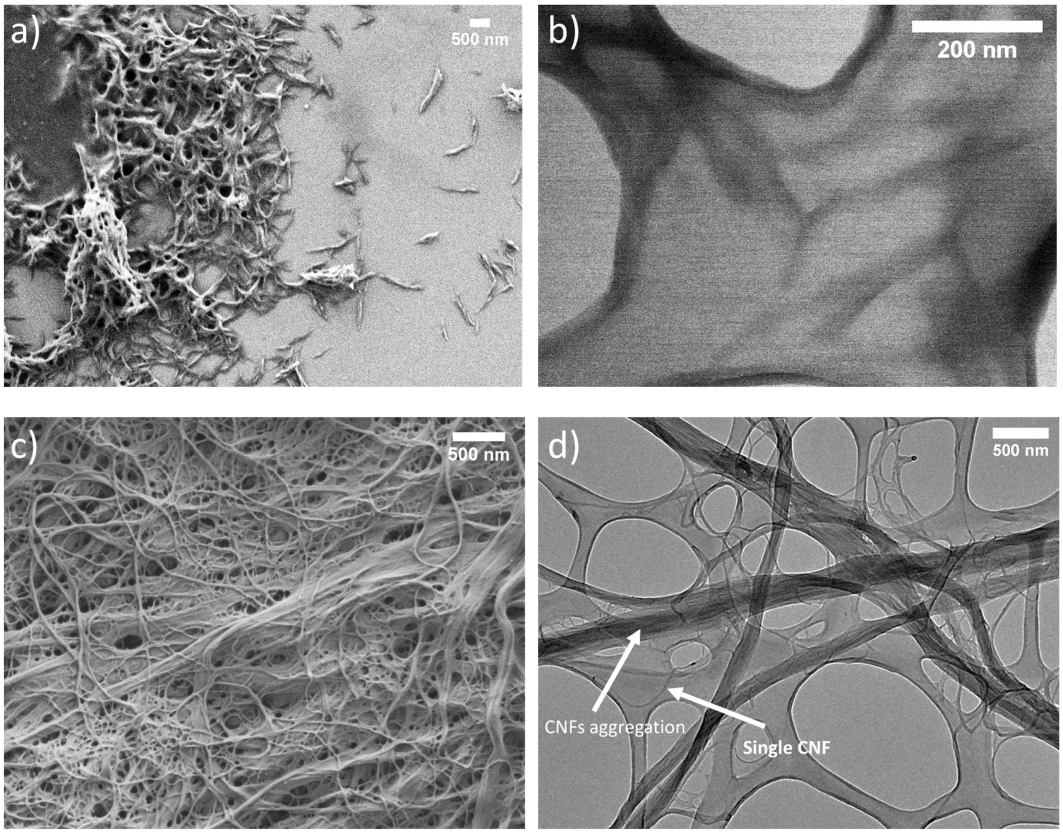

Figure 1. SEM and TEM micrographs of CNCs (a and b, respectively), SEM and TEM micrographs of CNFs (c and d, respectively).

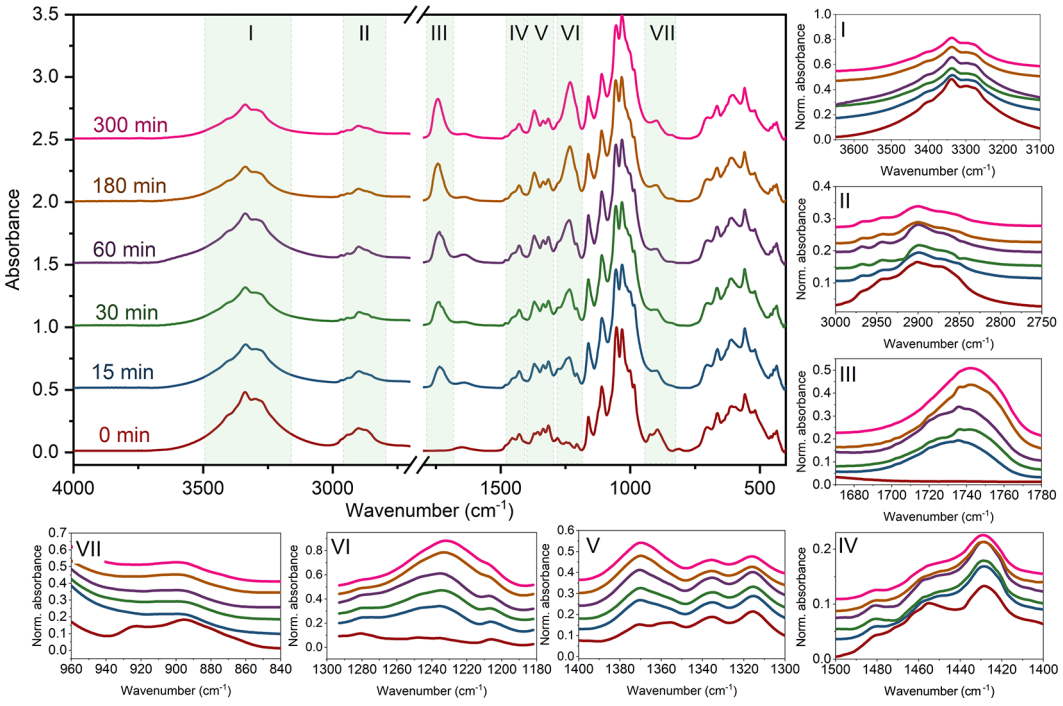

Figure 2. FT-IR spectra of unmodified and modified CNCs, with marked regions (I–VII) where change upon acetylation is observed. The peak at 1744 cm^{-1} is characteristic for acetyl bond and is proportional to acetyl content.

RESULTS AND DISCUSSION

Characterization Cellulose Nanomaterials. The morphological differences between the two tested materials were visible under SEM and TEM. The CNCs are in the form of rod-shaped particles that tend to aggregate, as visible in Figure 1a, with an average length of 294 ± 84 nm and width 11 nm ±5 nm (Figure 1b), which is in agreement with the literature.[31] On the other hand, CNFs are shaped as a long, fibrilous

https://doi.org/10.1021/acssuschemeng.2c04686
ACS Sustainable Chem. Eng. 2022, 10, 15480−15489

network with an average diameter of a single fibril being 17 nm ± 6 nm and length of more than 100 μm (Figure 1c,d). Additional TEM images with lower magnification can be found in the Supporting Information (Figure S2).

On the surface of cellulose nanomaterials, not all hydroxyl groups are accessible for reaction because of different nucleophilicity of the surface hydroxyl groups and aggregation of cellulose nanomaterials. For acetylation, the hydroxyl group on C_6 is the most reactive, followed by C_2 and C_3[44,45] (in our model, we study C_6 with cooperating adjacent C_2). The amount of accessible hydroxyl groups was determined indirectly by integrating the signals obtained by ^{31}P NMR for unreacted TMDP, internal standard NHND and water (Figure S3). The results point to higher availability of hydroxyl groups in CNCs (3.05 ± 0.075 $mmol_{OH}\ g^{-1}_{CNCs}$) than CNFs (2.7 ± 0.22 $mmol_{OH}\ g^{-1}_{CNFs}$), revealing that 16.4% of all hydroxyl groups in CNCs and 14.7% in CNFs are reactive and hence potentially available for modification, which is in agreement with the literature.[28] It has to be taken into account that the limitation of this method regarding CNFs applies as the material was freeze-dried before analysis, which could impact the hydrogen bonding and hydroxyl groups accessibility. The theoretically calculated hydroxyl groups on the surface of CNCs (calculated 17.8% of all hydroxyl groups) was in agreement with experimentally obtained values, while it was higher for CNFs (the obtained value was 28.2% of all OH groups). For the experimentally obtained value to match the theoretically calculated one, the crystallite size would have to be 8 nm. However, as previously described by Brand et al.,[28] the difference could be attributed to the agglomeration and entanglement of the fibrils, also visible in Figure 1, causing not all surface hydroxyl groups to be available for the reaction. The difference in availability of surface hydroxyl groups between the two materials can be reasoned according to differences in the morphology as CNFs are more entangled.[46]

To evaluate the structural changes upon functionalization, the treated samples were inspected with FTIR-ATR. All FTIR spectra contain the characteristic peak for cellulose, located at 1056 cm^{-1}, which remains unchanged throughout the modification. The absence of the peak positioned between 1810 and 1785 cm^{-1} corresponding to C═O stretching in acetic anhydride[47,48] points to successful elimination of reactant residues. Since there are no major differences between the materials, in Figure 2 only the time evolution of CNCs spectra is shown (see Figure S4 for ATR-FTIR spectra of CNFs).

Functionalization affects seven regions, marked with I−VII. In region I, a decline in the intensity of a broad peak between 3500 and 3150 cm^{-1}, corresponding to stretching of O−H bonds in alcohols, is observed, which indicates a substitution of hydroxyl groups. Similarly, acetylation decreases the peak around 2900 cm^{-1} (region II), which corresponds to a C−H alkane stretching, which was previously noted in the literature.[49] Regions III and VI are associated with the carbonyl C═O stretching and C−O stretching of the acetyl group, respectively, all implying an increase in the acetyl content. Furthermore, in region IV, the nonmodified sample exhibits two peaks related to H−C−H and O−C−H in-plane bending (at 1430 cm^{-1})[50] and C−H bending in the methylene group (1465 cm^{-1}), while in the modified sampled a new adjacent peak, corresponding to C−H bending in methylene group arises in-between (at 1450 cm^{-1}). C−H bending vibrations of the newly formed methyl group are also responsible for changes in spectra in region V.[49] Lastly, the peak between 940 and 860 cm^{-1} (region VII) belong to the alkane C−H bending.

A CP-MAS ^{13}C NMR analysis of pristine and functionalized CNCs (Figure 3a) and CNFs (Figure 3b) was carried out and

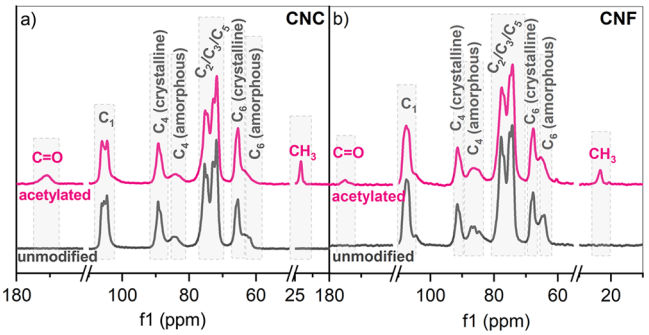

Figure 3. Representative CP MAS solid-state ^{13}C NMR spectra of (a) unmodified and acetylated CNCs (experiment 1.14); (b) unmodified and acetylated CNFs (experiment 2.7).

further confirmed successful grafting. All of the obtained spectra are characteristic for cellulose materials with well-defined peaks, corresponding to C1, C4, and C6 located at 105.7, 89.19, and 65.3 ppm for CNCs and 107.0, 91.5, and 67.6 ppm for CNFs, respectively, and overlapping signals for C2, C3, and C5 between 80−70 ppm. For CNFs, the C4 crystalline peak exhibits a lower intensity than for CNCs, pointing to lower crystallinity of CNFs, which is consistent with intrinsic properties of the materials. After the acetylation, new peaks centered at 175 and 23 ppm develop, corresponding to the C═O and CH_3 bonds, respectively, of the acetyl group. The peaks for C1 in CNCs additionally form a shoulder. No broadening of the peak for the C4 crystalline plane shows that the crystallinity does not change during the reaction.

The crystallinity of the samples was further inspected with XRD, revealing an initial 80% crystallinity in CNCs and a maximum loss of 4%, and a 77% crystallinity in CNFs with a maximum loss of 11% (Table S3 and Figures S5 & S6). Although it is reported in the literature that formation of allomorphs is possible,[51] the peak at 11.5° pointing to their existence is not present in this study.

Mechanism from First-Principles. Acetylation is generally described as a nucleophilic attack of the hydroxylic oxygen atom on the carbonylic carbon. A Lewis base, which can be pyridine, acetic anion or even water, abstracts the hydroxylic proton. The ensuing negatively charged intermediate loses an acetylic group, yielding the acetylated product. Since it is experimentally well-known that the C6 site is the most reactive for the nucleophilic attack,[44,45] we limit our theoretical investigations to the mechanism of 6OH acetylation. Electronic properties calculations (Fukui functions) showed that 2OH and 3OH are indeed less active (see Supporting Information).

This simplistic depiction is useful in predicting the reactivity of organic compounds but must be refined using quantum methods. First, we deal with the uncatalyzed reaction since no catalyst is present in our experimental setup.

During acetylation, a new C−O bond between the alcohol and acetyl forms, and a C−O bond in the acetic anhydride disintegrates. In a one-step mechanism, the rearrangements happen in a concerted fashion, while in the two-step

https://doi.org/10.1021/acssuschemeng.2c04686
ACS Sustainable Chem. Eng. 2022, 10, 15480−15489

mechanism a new bond form first and then the formed intermediate quickly decomposes. Both cases are accompanied by proton migration to any of the three oxygen atoms in the anhydride (see Figure 6).

We must also consider the involvement of the (sterically) adjacent hydroxyl groups. When the hydroxylic proton migrates, it can attach to the anhydride molecule directly or it can migrate to the neighboring hydroxylic group, whose proton moves to the anhydride. The latter transition state is lower in energy because the six- or eight-ring transition state is more stable than a four-ring transition state (*cf.* benzene and cyclobutadiene).[52] The 2-OH group from the adjacent monomeric unit is closest to the 6-OH group of the active monomeric unit (see Supporting Information). Since the energy difference between the gg, tg, and gt conformers is less than 1 kcal mol^{-1},[53] tg can transform to gg, which is sterically more accessible for the reaction with bulky nucleophiles.

Using pyridine to facilitate acetylation with acetic anhydride is analogous to the Steglich esterification,[54] where 4-(dimethylamino)pyridine[55] or imidazole[15] is used for acetylation of alcohols. We show the postulated mechanism in Figure 6. First (step 0), the acetylpyridinium (**AcPy**) ion as an active intermediate is formed in a reaction between the acetic anhydride (**AAn**) and pyridine (**Py**).[56] We calculate the activation barrier for this reaction at 34 kJ mol^{-1} acetate (**AA**) forming in the process.

The active intermediate (**AcPy**) then reacts with an accessible cellulose hydroxyl group. If its proton is transferred to the pyridinium nitrogen, the acetylation proceeds in one step (step 1) and yields acetylcellulose (**AC**) and a pyridinium ion (**PyH**). The proton is not directly transferred to the nitrogen atom, which would entail a barrier of >100 kJ mol^{-1} (not shown). Instead, the hydroxyl group from the adjacent monomeric unit chaperons the reaction, as depicted in Figure 4 in an exothermic reaction (ΔE = −78 kJ mol^{-1}) with an activation barrier of 56 kJ mol^{-1}.

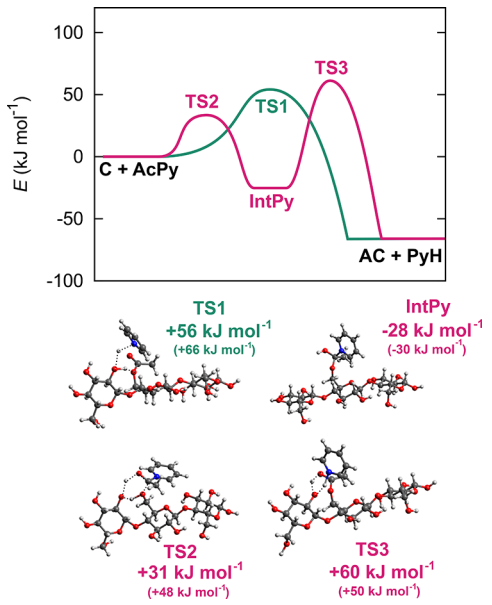

Figure 4. (top) Potential energy surface for acetylpyridinium-mediated acetylation of cellulose, and (bottom) intermediate and transition states with energies and Gibbs free energies (in parentheses) written. Note that the values are relative to **C** + **AcPy**.

This is expected since a direct proton transfer would occur in a four-member ring transition state, which is sterically strained. When an adjacent OH group participates, the transition state assumes a single-member ring structure, which is energetically more favorable. A similar effect was observed by Lawal et al.[52]

Alternatively, the hydroxylic proton atom can first bind to the carbonylic oxygen atom of the acetylpyridinium. This reaction step has a lower barrier (31 kJ mol^{-1}), producing an intermediate (**IntPy**) (step 2), which decomposes into acetylcellulose (**AC**) and a pyridinium ion (**PyH**) (step 3) after overcoming a barrier of 88 kJ mol^{-1}. Both proton transfers are mediated by a hydroxyl group from the adjacent monomeric unit (Figure 4).

Since **Py** and **PyH** quickly interconvert with acetic acid **AAH**/**AA** in a acid−base proton exchange, they are not differentiated in the model.

The activation barrier of the first step in the two-step mechanism is lower than that of the one-step mechanism, which is not true for the second step. Hence, both mechanisms must be accounted for in a microkinetic model. The calculated thermodynamic and kinetic parameters are summarized in Table 2 and used in the microkinetic model.

Table 2. Kinetic Parameters of the Elementary Reaction Steps as Labeled in Figure 6 as Determined by DFT and Refined by Regression Analysis of the Microkinetic Model

	DFT		Regression analysis	
Reaction step	ΔE(kJ mol^{-1})	E_a(kJ mol^{-1})	E_a(kJ mol^{-1})	A (s^{-1})
0	+32	34	33.5	1.56×10^{07}
1	−78	56	50.4	1.55×10^{04}
2	−28	31	34.1	6.06×10^{01}
3	−50	88	79.2	6.28×10^{06}

The reported values are from simulations using pyridine as the solvent in the SMD model. Additionally, the most probable reaction pathway was modeled using toluene as the solvent to ascertain if there is a noticeable difference in a pyridine/toluene mixture, which was used for CNFs. The toluene-calculated values were negligibly different (≤5%), which is expected because both solvents are rather apolar. This difference is smaller than the subsequent refinement of the DFT values in the regression analysis of the kinetic model and can thus be ignored.

Kinetics and Modeling. The acetyl content in the cellulose nanomaterials, from the ATR-FTIR spectra, was evaluated for varying reaction time and temperature, and reactants ratio. To eliminate the effect of transport on the acetylation, three mixing rates and different durations of CNCs pretreatment were tested. The obtained results are presented and discussed in Figures S7−S9.

CNCs generally allowed for a higher degree of acetylation under the same conditions compared to CNFs, as seen in Figure 5, which is consistent with a higher availability of hydroxyl groups for the reaction on the surface; however, dilution due to the presence of a solvent (toluene) in CNFs acetylation has to be taken into account. The grafting efficiency increases with the reaction temperature in CNCs modification, and the highest acetyl content was obtained at 90 °C (94% of the hydroxyl groups accessible for reaction, experiment 1.12). To the contrary, 70 °C was shown to be optimal for the acetylation of CNFs, reaching 72% of accessible hydroxyl

https://doi.org/10.1021/acssuschemeng.2c04686
ACS Sustainable Chem. Eng. 2022, 10, 15480−15489

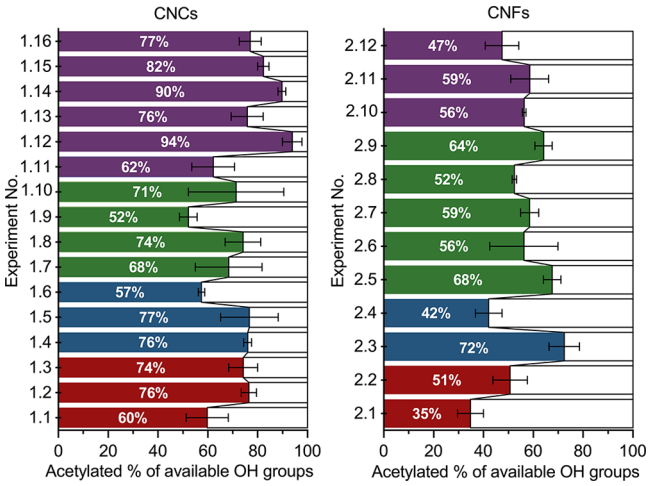

Figure 5. Proportion of acetylated groups relative to accessible hydroxyl groups on the surface, as determined in this study. The experiment numbers refer to Table 1. For clarity, bars are color-coded: red (60 °C), blue (70 °C), green (80 °C), violet (90 °C).

groups (experiment 2.3), while the acetyl content began to decrease with higher temperature (2.5−2.12), which could be attributed to the temperature approaching the boiling point of the solvent toluene (110.6 °C). As the role of toluene is to prevent aggregation of fibers, its shift to gaseous phase might cause lower availability of hydroxyl groups on the surface. Further testing of different reactant ratios (between concentrations of acetic anhydride and pyridine relative to cellulose nanomaterial) revealed the negative influence of higher pyridine concentration for the acetylation of CNCs, due to the dilution of the reaction media and consequent shift of the dependency of the reaction rate onto the reactant transfer to the surface of cellulose nanomaterials (experiments 1.5, 1.6, 1.8, 1.9, 1.14, 1.15, 1.16). On the other hand, an increase in the relative concentration of acetic anhydride improves esterification (1.13, 1.14, 2.6, 2.7).

Using microkinetic modeling with DFT input, reaction kinetic constants and activation energies for the individual functionalization steps on the cellulose nanomaterials surface were obtained. The microkinetic model was constructed as a system of differential equations (see Supporting Information), describing the reactions from the mechanism, shown in Figure 6.

The reaction rate is the highest in the first 60 min and then plateaus, regardless of the cellulose nanomaterial or the conditions used (Figure 7). An increase in the amount of pyridine added to the reaction mixture adversely affects the initial reaction rate for CNCs surface modification, indicating that the kinetics is controlled by the acetic anhydride concentration. However, this effect is not as noticeable during CNFs functionalization. At longer reaction times, a slight decrease in the acetyl content in CNFs was observed in experiments with AGU:pyridine ratio 1:30 (experiments 2.1, 2.6, and 2.11), indicating that the overall reaction might be reversible in the presence of the solvent, which has been proposed by Chunilall et al.[57]

While DFT-derived data were used as an initial guess for the microkinetic model, the inherent approximations in the model mean that they should be further refined for a problem at hand. Using regression analysis, as described in a previous section, we obtained the optimized values which are listed in Table 2. Additionally, the temperature-independent pre-exponential factors (A_i) were back-calculated from the determined (temperature-dependent) reaction rates and (temperature-independent) activation barriers. The values for a single-step reaction reported in the literature are slightly lower (41.6 and 39 kJ mol^{-1}); however, the acetylation was carried out on wood blocks.[24,58]

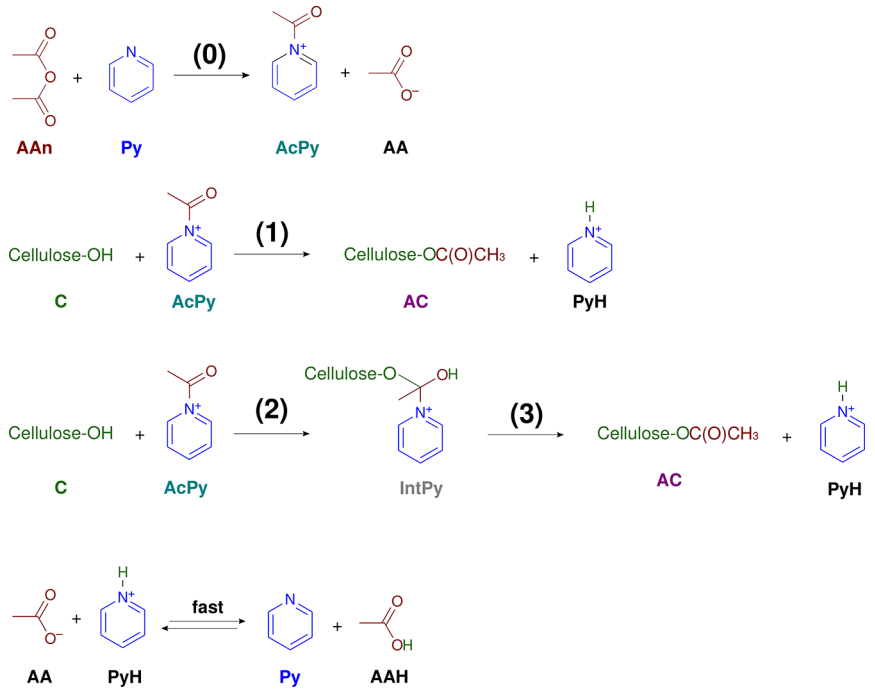

Figure 6. Mechanism of pyridine-mediated acetylation with acetic anhydride with labeled relevant reaction steps (0−3) and fast interconversion of **PyH** and **Py** that is not differentiated in the model.

https://doi.org/10.1021/acssuschemeng.2c04686
ACS Sustainable Chem. Eng. 2022, 10, 15480−15489

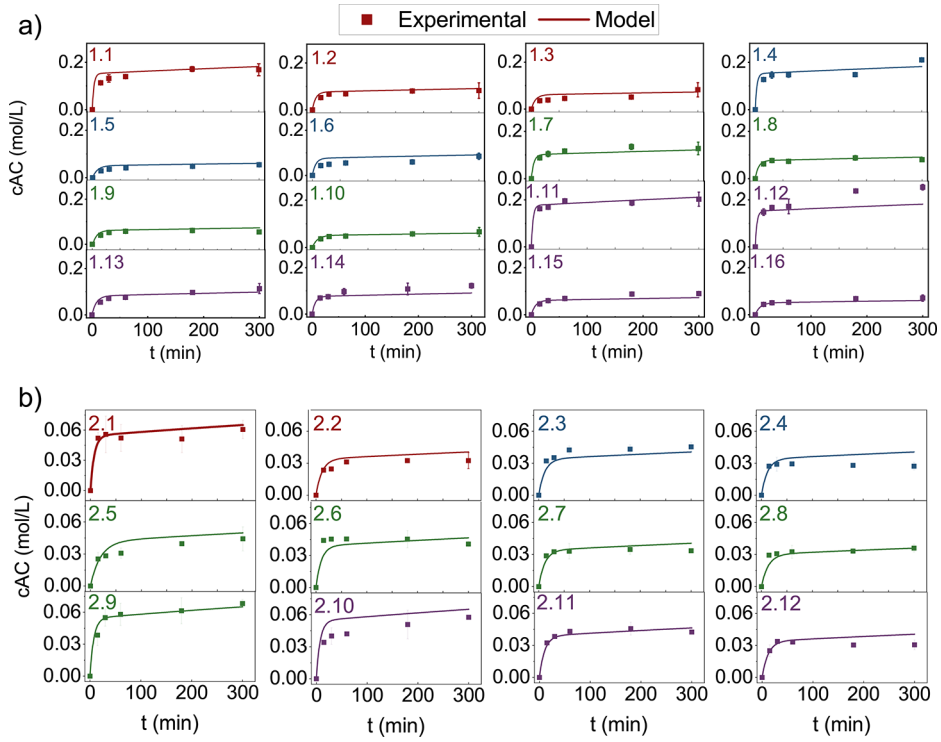

Figure 7. Experimental and model values of (a) CNCs acetylation and (b) CNFs acetylation. The plots are color-coded by temperature: red (60 °C), blue (70 °C), green (80 °C), violet (90 °C).

CONCLUSIONS

In this work, the hypothesis of a revised mechanism for acetylation of two cellulose nanomaterials (CNCs and CNFs) with acetic anhydride in the presence of pyridine was confirmed. Computation suggested that the reactions proceeds via two competitive mechanisms. The active species (acetylpyridinium ion) must first form, which then reacts with accessible cellulose hydroxyl groups. The calculated kinetic parameters (activation barriers) served as a skeleton for the developed microkinetic model, which described the experimental results and, through regression analysis, honed in on the true kinetic parameters.

ASSOCIATED CONTENT

Supporting Information

The Supporting Information is available free of charge at https://pubs.acs.org/doi/10.1021/acssuschemeng.2c04686.

Additional experimental methods, characterization (^{31}P NMR, FTIR, XRD, degrees of substitution, surface free energy) and detailed explanation of the kinetic model (PDF)

AUTHOR INFORMATION

Corresponding Author

Uroš Novak − *Department of Catalysis, Chemical Reaction Engineering, SI-1000 Ljubljana, Slovenia;* orcid.org/0000-0003-0561-8427; Phone: +386 (0)1 4760 283; Email: uros.novak@ki.si

Authors

Ana Oberlintner − *Department of Catalysis, Chemical Reaction Engineering, SI-1000 Ljubljana, Slovenia; Jožef Stefan International Postgraduate School, SI-1000 Ljubljana, Slovenia*

Matej Huš − *Department of Catalysis, Chemical Reaction Engineering, SI-1000 Ljubljana, Slovenia; Association for Technical Culture of Slovenia (ZOTKS), SI-1000 Ljubljana, Slovenia; University of Nova Gorica, SI-5000 Nova Gorica, Slovenia;* orcid.org/0000-0002-8318-5121

Blaž Likozar − *Department of Catalysis, Chemical Reaction Engineering, SI-1000 Ljubljana, Slovenia;* orcid.org/0000-0001-7226-4302

Complete contact information is available at: https://pubs.acs.org/10.1021/acssuschemeng.2c04686

Notes

The authors declare no competing financial interest.

ACKNOWLEDGMENTS

Sappi is acknowledged for the generous donation of Valida S. The authors are grateful to Dr. Anže Prašnikar for SEM imaging, Dr. Goran Dražić for TEM imaging, and Žan Lavrič for help with the microkinetic model development. This research was funded by a Ph.D. grant from the Slovenian Research Agency (Ana Oberlintner). M.H. thanks the Slovenian Research Agency (project funding J1-3020, core funding P2-0421, infrastructure funding I0-0039). The authors also acknowledge the financial support from the Slovenian Research Agency (research core funding No. P2-0152).

REFERENCES

(1) Lv, D.; Du, H.; Che, X.; Wu, M.; Zhang, Y.; Liu, C.; Nie, S.; Zhang, X.; Li, B. Tailored and Integrated Production of Functional Cellulose Nanocrystals and Cellulose Nanofibrils via Sustainable Formic Acid Hydrolysis: Kinetic Study and Characterization. *ACS Sustainable Chem. Eng.* **2019**, 7, 9449−9463.

(2) *Sandard Terms and Their Definition for Cellulose Nanomaterial*; TAPPI, 2022; https://www.tappi.org/content/hide/draft3.pdf.
(3) Gamelas, J. A.; Pedrosa, J.; Lourenço, A. F.; Mutjé, P.; González, I.; Chinga-Carrasco, G.; Singh, G.; Ferreira, P. J. On the morphology of cellulose nanofibrils obtained by TEMPO-mediated oxidation and mechanical treatment. *Micron* **2015**, *72*, 28−33.
(4) Heinze, T. Cellulose: Structure and Properties. *Cellulose Chemistry and Properties: Fibers, Nanocelluloses and Advanced Materials. Advances in Polymer Science* **2016**, *271*, 1−52.
(5) Habibi, Y.; Lucia, L. A.; Rojas, O. J. Cellulose Nanocrystals: Chemistry, Self-Assembly, and Applications. *Chem. Rev.* **2010**, *110*, 3479−3500.
(6) Tardy, B. L.; Mattos, B. D.; Otoni, C. G.; Beaumont, M.; Majoinen, J.; Kämäräinen, T.; Rojas, O. J. Deconstruction and Reassembly of Renewable Polymers and Biocolloids into Next Generation Structured Materials. *Chem. Rev.* **2021**, *121*, 14088−14188.
(7) Wickholm, K.; Larsson, P. T.; Iversen, T. Assignment of non-crystalline forms in cellulose I by CP/MAS 13C NMR spectroscopy. *Carbohydr. Res.* **1998**, *312*, 123−129.
(8) Miao, C.; Hamad, W. Y. Cellulose reinforced polymer composites and nanocomposites: a critical review. *Cellulose* **2013**, *20*, 2221−2262.
(9) Oksman, K.; Aitomäki, Y.; Mathew, A. P.; Siqueira, G.; Zhou, Q.; Butylina, S.; Tanpichai, S.; Zhou, X.; Hooshmand, S. Review of the recent developments in cellulose nanocomposite processing. *Composites Part A: Applied Science and Manufacturing* **2016**, *83*, 2−18. Special Issue on Biocomposites
(10) Shojaeiarani, J.; Bajwa, D. S.; Stark, N. M. Green esterification: A new approach to improve thermal and mechanical properties of poly(lactic acid) composites reinforced by cellulose nanocrystals. *J. Appl. Polym. Sci.* **2018**, *135*, 46468.
(11) Espino-Pérez, E.; Domenek, S.; Belgacem, N.; Sillard, C.; Bras, J. Green process for chemical functionalization of nanocellulose with carboxylic acids. *Biomacromolecules* **2014**, *15*, 4551−4560.
(12) Wang, L.; Gardner, D. J.; Wang, J.; Yang, Y.; Tekinalp, H. L.; Tajvidi, M.; Li, K.; Zhao, X.; Neivandt, D. J.; Han, Y.; Ozcan, S.; Anderson, J. Towards industrial-scale production of cellulose nanocomposites using melt processing: A critical review on structure-processing-property relationships. *Composites Part B: Engineering* **2020**, *201*, 108297.
(13) Eyley, S.; Thielemans, W. Imidazolium grafted cellulose nanocrystals for ion exchange applications. *Chem. Commun.* **2011**, *47*, 4177−4179.
(14) Sèbe, G.; Ham-Pichavant, F.; Pecastaings, G. Dispersibility and Emulsion-Stabilizing Effect of Cellulose Nanowhiskers Esterified by Vinyl Acetate and Vinyl Cinnamate. *Biomacromolecules* **2013**, *14*, 2937−2944.
(15) Beaumont, M.; Jusner, P.; Gierlinger, N.; King, A. W. T.; Potthast, A.; Rojas, O. J.; Rosenau, T. Unique reactivity of nanoporous cellulosic materials mediated by surface-confined water. *Nat. Commun.* **2021**, *12*, 2513.
(16) Beaumont, M.; Tardy, B. L.; Reyes, G.; Koso, T. V.; Schaubmayr, E.; Jusner, P.; King, A. W. T.; Dagastine, R. R.; Potthast, A.; Rojas, O. J.; Rosenau, T. Assembling Native Elementary Cellulose Nanofibrils via a Reversible and Regioselective Surface Functionalization. *J. Am. Chem. Soc.* **2021**, *143*, 17040−17046.
(17) Ávila Ramírez, J. A.; Fortunati, E.; Kenny, J. M.; Torre, L.; Foresti, M. L. Simple citric acid-catalyzed surface esterification of cellulose nanocrystals. *Carbohydr. Polym.* **2017**, *157*, 1358−1364.
(18) Lin, N.; Huang, J.; Chang, P. R.; Feng, J.; Yu, J. Surface acetylation of cellulose nanocrystal and its reinforcing function in poly(lactic acid). *Carbohydr. Polym.* **2011**, *83*, 1834−1842.
(19) Jamaluddin, N.; Kanno, T.; Asoh, T.-A.; Uyama, H. Surface modification of cellulose nanofiber using acid anhydride for poly(lactic acid) reinforcement. *Materials Today Communications* **2019**, *21*, 100587.
(20) Swartz, J. L.; Li, R. L.; Dichtel, W. R. Incorporating Functionalized Cellulose to Increase the Toughness of Covalent Adaptable Networks. *ACS Appl. Mater. Interfaces* **2020**, *12*, 44110−44116.
(21) Sulbarán-Rangel, B.; Diaz, A. J. H.; Guzmán, A. C. G.; Rojas, O. J. Partially acetylated cellulose nanofibrils from Agave tequilana bagasse and Pickering stabilization. *J. Dispersion Sci. Technol.* **2022**, 1−9.
(22) Oberlintner, A.; Likozar, B.; Novak, U. Hydrophobic functionalization reactions of structured cellulose nanomaterials: Mechanisms, kinetics and in silico multi-scale models. *Carbohydr. Polym.* **2021**, *259*, 117742.
(23) Chen, M.; Li, R.-M.; Runge, T.; Feng, J.; Feng, J.; Hu, S.; Shi, Q.-S. Solvent-Free Acetylation of Cellulose by 1-Ethyl-3-methylimidazolium Acetate-Catalyzed Transesterification. *ACS Sustainable Chem. Eng.* **2019**, *7*, 16971−16978.
(24) Minato, K.; Ito, Y. Analysis of the factors influencing the acetylation rate of wood. *Journal of Wood Science* **2004**, *50*, 519−523.
(25) Luo, P.; Cao, C.; Liang, Y.; Ma, X.; Xin, C.; Jiao, Z.; Cao, J.; Zhang, J. Kinetic Study of the Acetylation of Cotton Linter Pulp. *BioResources* **2013**, *8*, 2708−2718.
(26) Ramsden, M. J.; Blake, F. S. R.; Fey, N. J. The effect of acetylation on the mechanical properties, hydrophobicity, and dimensional stability ofPinus sylvestris. *Wood Science and Technology* **1997**, *31*, 97−104.
(27) Kanematsu, Y.; Kikuchi, Y.; Yano, H. Life Cycle Greenhouse Gas Emissions of Acetylated Cellulose Nanofiber-Reinforced Polylactic Acid Based on Scale-Up from Lab-Scale Experiments. *ACS Sustainable Chem. Eng.* **2021**, *9*, 10444−10452.
(28) Brand, J.; Pecastaings, G.; Sèbe, G. A versatile method for the surface tailoring of cellulose nanocrystal building blocks by acylation with functional vinyl esters. *Carbohydr. Polym.* **2017**, *169*, 189−197.
(29) Peng, Y.; Gardner, D. J.; Han, Y.; Kiziltas, A.; Cai, Z.; Tshabalala, M. A. Influence of drying method on the material properties of nanocellulose I: thermostability and crystallinity. *Cellulose* **2013**, *20*, 2379−2392.
(30) Segal, L.; Creely, J. J.; Martin, J. A.; Conrad, C. M. An Empirical Method for Estimating the Degree of Crystallinity of Native Cellulose Using the X-Ray Diffractometer. *Text. Res. J.* **1959**, *29*, 786−794.
(31) Kunaver, M.; Anžlovar, A.; Žagar, E. The fast and effective isolation of nanocellulose from selected cellulosic feedstocks. *Carbohydr. Polym.* **2016**, *148*, 251−258.
(32) Tingaut, P.; Zimmermann, T.; Lopez-Suevos, F. Synthesis and characterization of bionanocomposites with tunable properties from poly(lactic acid) and acetylated microfibrillated cellulose. *Biomacromolecules* **2010**, *11*, 454−464.
(33) Valiev, M.; Bylaska, E.J.; Govind, N.; Kowalski, K.; Straatsma, T.P.; Van Dam, H.J.J.; Wang, D.; Nieplocha, J.; Apra, E.; Windus, T.L.; de Jong, W.A. NWChem: A comprehensive and scalable open-source solution for large scale molecular simulations. *Comput. Phys. Commun.* **2010**, *181*, 1477−1489.
(34) Zhao, Y.; Truhlar, D. G. The M06 suite of density functionals for main group thermochemistry, thermochemical kinetics, noncovalent interactions, excited states, and transition elements: two new functionals and systematic testing of four M06-class functionals and 12 other function. *Theor. Chem. Acc.* **2008**, *120*, 215−241.
(35) Krishnan, R.; Binkley, J. S.; Seeger, R.; Pople, J. A. Self-consistent molecular orbital methods. XX. A basis set for correlated wave functions. *J. Chem. Phys.* **1980**, *72*, 650−654.
(36) Clark, T.; Chandrasekhar, J.; Spitznagel, G. W.; Schleyer, P. V. R. Efficient diffuse function-augmented basis sets for anion calculations. III. The 3-21+G basis set for first-row elements, Li−F. *J. Comput. Chem.* **1983**, *4*, 294−301.
(37) Frisch, M. J.; Pople, J. A.; Binkley, J. S. Self-consistent molecular orbital methods 25. Supplementary functions for Gaussian basis sets. *J. Chem. Phys.* **1984**, *80*, 3265−3269.
(38) McLean, A. D.; Chandler, G. S. Contracted Gaussian basis sets for molecular calculations. I. Second row atoms, Z = 11−18. *J. Chem. Phys.* **1980**, *72*, 5639−5648.

(39) Walker, M.; Harvey, A. J. A.; Sen, A.; Dessent, C. E. H. Performance of M06, M06-2X, and M06-HF Density Functionals for Conformationally Flexible Anionic Clusters: M06 Functionals Perform Better than B3LYP for a Model System with Dispersion and Ionic Hydrogen-Bonding Interactions. *J. Phys. Chem. A* **2013**, *117*, 12590−12600.
(40) Marenich, A. V.; Cramer, C. J.; Truhlar, D. G. Universal Solvation Model Based on Solute Electron Density and on a Continuum Model of the Solvent Defined by the Bulk Dielectric Constant and Atomic Surface Tensions. *J. Phys. Chem. B* **2009**, *113*, 6378−6396.
(41) Zarkevich, N. A.; Johnson, D. D. Nudged-elastic band method with two climbing images: Finding transition states in complex energy landscapes. *J. Chem. Phys.* **2015**, *142*, 24106.
(42) Ponnuchamy, V.; Sandak, A.; Sandak, J. Multiscale modelling investigation of wood modification with acetic anhydride. *Phys. Chem. Chem. Phys.* **2020**, *22*, 28448−28458.
(43) Paajanen, A.; Ceccherini, S.; Maloney, T.; Ketoja, J. A. Chirality and bound water in the hierarchical cellulose structure. *Cellulose* **2019**, *26*, 5877−5892.
(44) Goodlett, V. W.; Dougherty, J. T.; Patton, H. W. Characterization of cellulose acetates by nuclear magnetic resonance. *Journal of Polymer Science Part A-1: Polymer Chemistry* **1971**, *9*, 155−161.
(45) Miyamoto, T.; Sato, Y.; Shibata, T.; Tanahashi, M.; Inagaki, H. 13C-NMR spectral studies on the distribution of substituents in water-soluble cellulose acetate. *Journal of Polymer Science: Polymer Chemistry Edition* **1985**, *23*, 1373−1381.
(46) Doyle, S.; Pethrick, R. A.; Harris, R. K.; Lane, J. M.; Packer, K. J.; Heatley, F. 13C nuclear magnetic resonance studies of cellulose acetate in the solution and solid states. *Polymer* **1986**, *27*, 19−24.
(47) Wallace, E. W. Infrared Spectra by NIST Mass Spectrometry Data Center. https://www.nist.gov/mml/biomolecular-measurement/mass-spectrometry-data-center, 2022.
(48) Muhammad Djuned, F.; Asad, M.; Mohamad Ibrahim, M. N.; Wan Daud, W. R. Synthesis and Characterization of Cellulose Acetate from TCF Oil Palm Empty Fruit Bunch Pulp. *BioResources* **2014**, *9*, 4710−4721.
(49) Fei, P.; Liao, L.; Cheng, B.; Song, J. Quantitative analysis of cellulose acetate with a high degree of substitution by FTIR and its application. *Analytical Methods* **2017**, *9*, 6194−6201.
(50) Proniewicz, L. M.; Paluszkiewicz, C.; Wesełucha-Birczyńska, A.; Majcherczyk, H.; Barański, A.; Konieczna, A. FT-IR and FT-Raman study of hydrothermally degradated cellulose. *J. Mol. Struct.* **2001**, *596*, 163−169.
(51) Operamolla, A.; Casalini, S.; Console, D.; Capodieci, L.; Di Benedetto, F.; Bianco, G. V.; Babudri, F. Tailoring water stability of cellulose nanopaper by surface functionalization. *Soft Matter* **2018**, *14*, 7390−7400.
(52) Lawal, M. M.; Govender, T.; Maguire, G. E. M.; Honarparvar, B.; Kruger, H. G. Mechanistic investigation of the uncatalyzed esterification reaction of acetic acid and acid halides with methanol: a DFT study. *J. Mol. Model.* **2016**, *22*, 235.
(53) Klewinghaus, P.; van Eijck, B. P.; Kouwijzer, M. L. C. E.; Kroon, J. Molecular dynamics study of conformational equilibria in aqueous d-glucose and d-galactose. *Journal of Molecular Structure: THEOCHEM* **1997**, *395*−*396*, 289−295.
(54) Neises, B.; Steglich, W. Simple Method for the Esterification of Carboxylic Acids. *Angewandte Chemie International Edition in English* **1978**, *17*, 522−524.
(55) Xu, S.; Held, I.; Kempf, B.; Mayr, H.; Steglich, W.; Zipse, H. The DMAP-Catalyzed Acetylation of Alcohols—A Mechanistic Study (DMAP = 4-(Dimethylamino)pyridine). *Chem. Eur. J.* **2005**, *11*, 4751−4757.
(56) Fersht, A. R.; Jencks, W. P. Acetylpyridinium ion intermediate in pyridine-catalyzed acyl transfer. *J. Am. Chem. Soc.* **1969**, *91*, 2125−2126.
(57) Chunilall, V.; Bush, T.; Larsson, P. T.; Iversen, T.; Kindness, A. A CP/MAS 13C-NMR study of cellulose fibril aggregation in eucalyptus dissolving pulps during drying and the correlation between aggregate dimensions and chemical reactivity. *Holzforschung* **2010**, *64*, 693−698.
(58) Hill, C. A. S.; Jones, D.; Strickland, G.; Cetin, N. S. Kinetic and Mechanistic Aspects of the Acetylation of Wood with Acetic Anhydride. *Holzforschung* **1998**, *52*, 623−629.